International Journal for Research in Engineering Application & Management (IJREAM)
ISSN : 2454-9150 Vol-09, Issue-07, Oct 2023

DVT Grown Hexagonal Tungsten Sulphoselenide Single Crystals for Advanced Photo Detection Application

Ankit G. Dalvaniya[a,*], Shubham Umeshkumar Gupta[a,b], Chaitanya Limberkar[a,c], Kireetkumar D. Patel[a **]

[a]Thin Film Device Fabrication & Characterisation Laboratory, Department of Physics, Sardar Patel University, Vallabh Vidyanagar, Gujarat, India

[b]Department of Material Science, Sardar Patel University, Vallabh Vidyanagar, Gujarat, India

[c]Department of Physics, The M. S. University of Baroda, Pratapgunj, Vadodara, Gujarat, India

Corresponding authors: *ankitgd1995@gmail.com (Ankit G. Dalvaniya), **kdptflspu@gmail.com (Kireetkumar D. Patel)

Abstract. - Transition metal dichalcogenide (TMDC) materials are well-known as highly photosensitive materials. In this article, substitution of sulphur in WSe_2 with different proportion along with optoelectronic properties of WS_xSe_{2-x} (x = 0.0, 1.0, 1.5, 2.0) single crystals (SCs) grown by direct vapour transport technique are studied. The elemental composition and purity of the grown crystals were determined by the energy-dispersive X-ray analysis (EDAX). Powder X-ray diffraction (PXRD) and selected area electron diffraction (SAED) results revealed alloy's crystallinity and hexagonal lattice structure. The layered structures of the grown crystals were examined with the aid of a optical microscope and scanning electron microscope (SEM). High-resolution transmission electron microscopy (HRTEM) analysis was also carried out to demonstrate the hexagonal crystalline nature of the alloy crystals. The peak shifting towards higher 2θ in PXRD suggests the successful substitution of sulphur for a selenium atom in grown crystals. The substitution is confirmed by the blue shift of the A_{1g} vibrational mode in Raman spectroscopy. The optoelectronic property of the WS_xSe_{2-x} (x=0.0, 1.0, 1.5, 2.0) SCs is studied by fabricating a crystal-based photo-detector and examined time-resolved photo response under visible radiations of different incident wavelengths at room temperature. WS_xSe_{2-x} (x=0.0, 1.0, 1.5, 2.0) single crystals are found to be decent photo detectors for development of future optoelectronic devices.

Keywords – DVT, Crystals, Photo.

I. INTRODUCTION

Two-dimensional (2D) materials such as TMDC materials have gained a lot of interest in research field in recent years [1-4]. The immense potential of TMDCs has led considerable interest in the investigation of additional layered nanostructures that can balance the need for 2D materials. TMDCs often exhibit semi-metallic properties, so it is very important to form semiconducting and insulating 2D layered materials [5-9]. 2D TMDC materials exhibit structurally similar characteristics to graphene, so that it can be incorporated to form variety of compounds as per material science perspective [10]. Moreover, the band gap of TMDC materials can be well altered by various techniques. In reality, when the TMDC material is sliced into only one or few layered crystalline structures, band gap of many of them shows significant change [11]. Furthermore, among from semiconducting TMDCs, especially MoS_2, WS_2, $MoSe_2$ and WSe_2 are materials which are studied extensively [12,13].

Tungsten sulphoselenides (WS_xSe_{2-x}) is considered to be one of the finest material series from TMDC material class because it has drawn the great amount of interest owing itself due to its tunable as well as visible region enabled band gap that have prospective use in photovoltaic devices, photonic, and semiconductor heterostructures [14,15]. Herein, physical properties along with optoelectronic property of WS_xSe_{2-x} (x=0.0, 1.0, 1.5, 2.0) single crystals are critically explored and discussed in terms of photo detector parameters such as responsivity and detectivity.

II. EXPERIMENTAL DETAILS.

2.1 Crystal growth.

Dual zone furnace was used for crystal growth. Here, one zone is called the source zone and the other zone is called the growth zone [16,17]. The ampoule is kept horizontally in the dual zone furnace. It was given proper temperature according to the melting point of the growth material by using the temperature controller. The temperature profile of crystal growth is divided in three parts. In the first part, source zone and growth zone are brought to 1373 K and 1333 K at a rate of 30 K/h respectively. In the second part, both zones are kept at higher temperature constantly with this temperature gradient for 70 hours. In the third cycle, it

 DOI : 10.35291/2454-9150.2023.0200

is cooled down to room temperature at the rate of 30 K/h. Due to the temperature difference between source zone and growth zone, the vaporized compound material was transferred from the source zone to the growth zone and the crystal formation begins at growth zone. At the end of this process of crystal growth, irregularly shaped shiny crystals having thickness of about 10-20 μm are collected from ampoule.

2.2 Material characterisations.

The as-grown crystals of WS_xSe_{2-x} (x=0.0, 1.0, 1.5, 2.0) were first characterized by EDAX analysis for determining elemental purity and chemical stoichiometric proportion. Surface topology was studied by a Carl-Zeiss optical microscope and scanning electron microscope (SEM). The phase identification, unit cell parameter and crystallinity of the crystals were observed by powder XRD using Cu-Kα radiation. High-resolution transmission electron microscopy (HRTEM) and selected area electron diffraction (SAED) were employed to verify the crystallinity of the ternary alloys. The vibrational properties of the crystals were studied by Raman spectroscopy.

2.3 Photodetection property.

Optoelectronic properties of ternary alloy crystals were studied by fabricating WS_xSe_{2-x} (x=0.0, 1.0, 1.5, 2.0) SC-based photodetectors. The crystals were mechanically cleaved with the aid of scotch tape, cleaned with acetone and fixed on a mica sheet. Two copper wires were bonded with the help of conductive silver paste which acts as contacts for the photodetector. The fabricated sample was kept in a vacuum oven at a temperature of 50°C for 3 hours to dry in the silver paste contact. The fabricated photodetector was then exposed to various incident visible radiations and the time-resolved photo response was recorded using Keithley 4200 semiconductor characterization system (SCS).

III. RESULTS AND DISCUSSION.

Chemical composition and determination of elements present in the grown samples were carried out by energy dispersive analysis of X-ray (EDAX) [18]. The EDAX spectrum shown in Figure1 (a-d) depicts different peaks corresponding to the binding energy of respective electrons present in each element in the grown crystal such as W, S, and Se. There is no extra peak detected so it is concluded that the formed crystals don't have any type of impurities in it. The surface texture was studied through an optical microscope. The optical microscope images are shown in Figure 2 (a-d) in which it is noticed that grown crystals are arranged in a layer typed structure. Furthermore, micro hexagonal flakes are also observed in the crystals so it is confirmed that the grown crystals exhibit hexagonal structure. Figure 2 (d) illustrates spiral hexagonal arrangement of the grown crystal due to the screw dislocation mechanism. The surface morphology of grown crystals was studied by using scanning electron microscope on a length scale of 10 μm by using their topography modes as shown in Figure 3 (a–d). These Figure 3 (d) shows a high magnification and a large depth field of hexagonal flakes on the crystal surface. It is also noticed that hexagonal flakes are arranged in layered manner. This layered property is accountable for anisotropy of grown alloys.

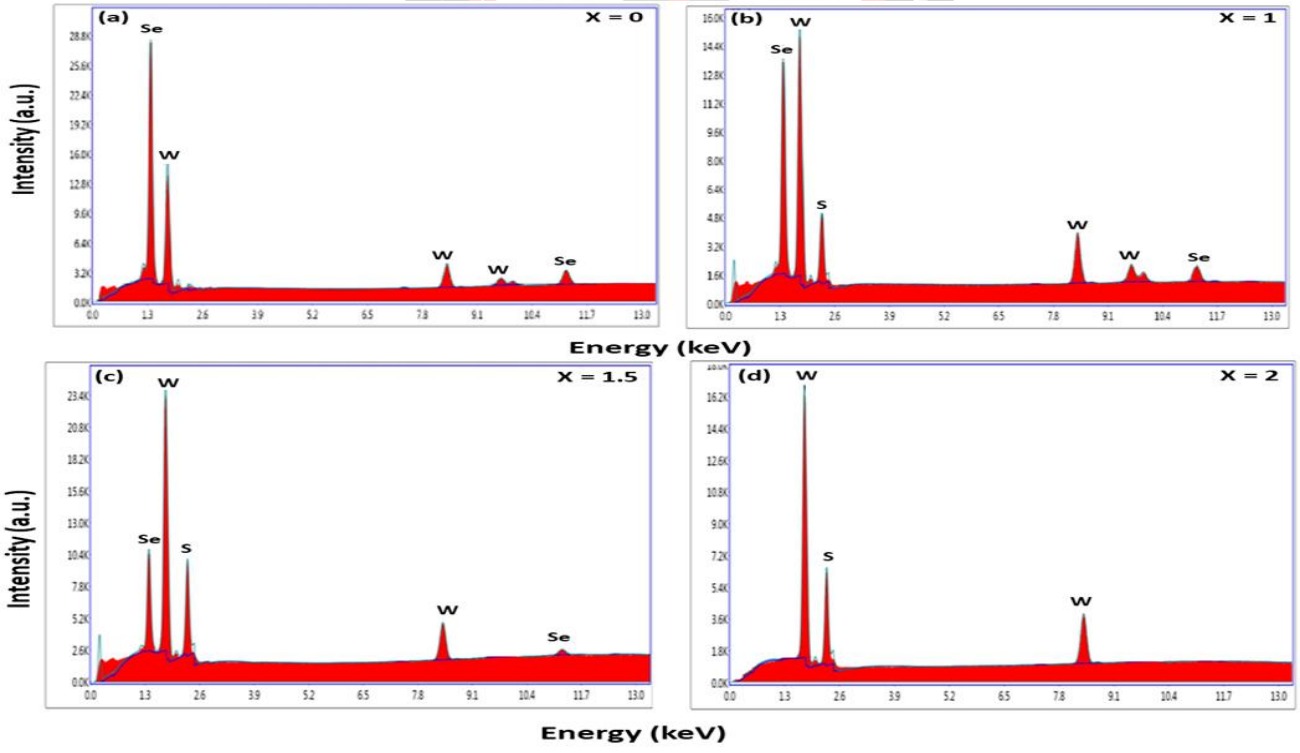

Figure 1. Energy dispersive analysis of X-ray (EDAX) spectrum of (a) WSe2 (b) WSSe (c) WS1.5Se0.5 (d) WS2 SCs.

 DOI : 10.35291/2454-9150.2023.0200

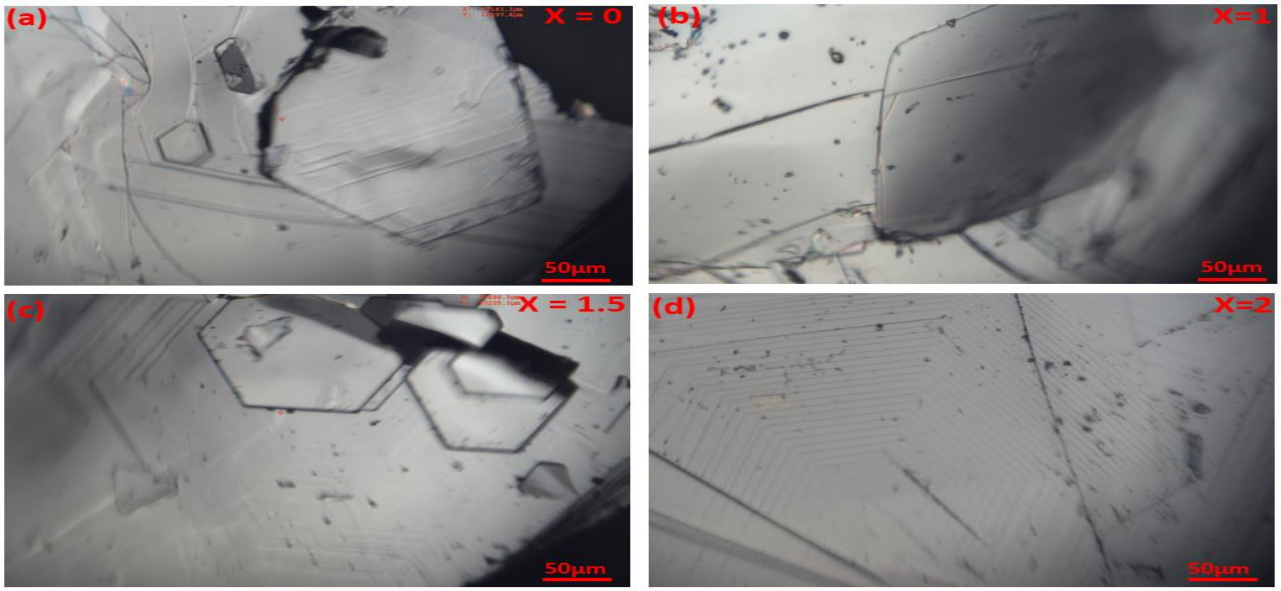

Figure 2. Optical micrographs of WSxSe2-x (x=0.0, 1.0, 1.5, 2.0) SCs.

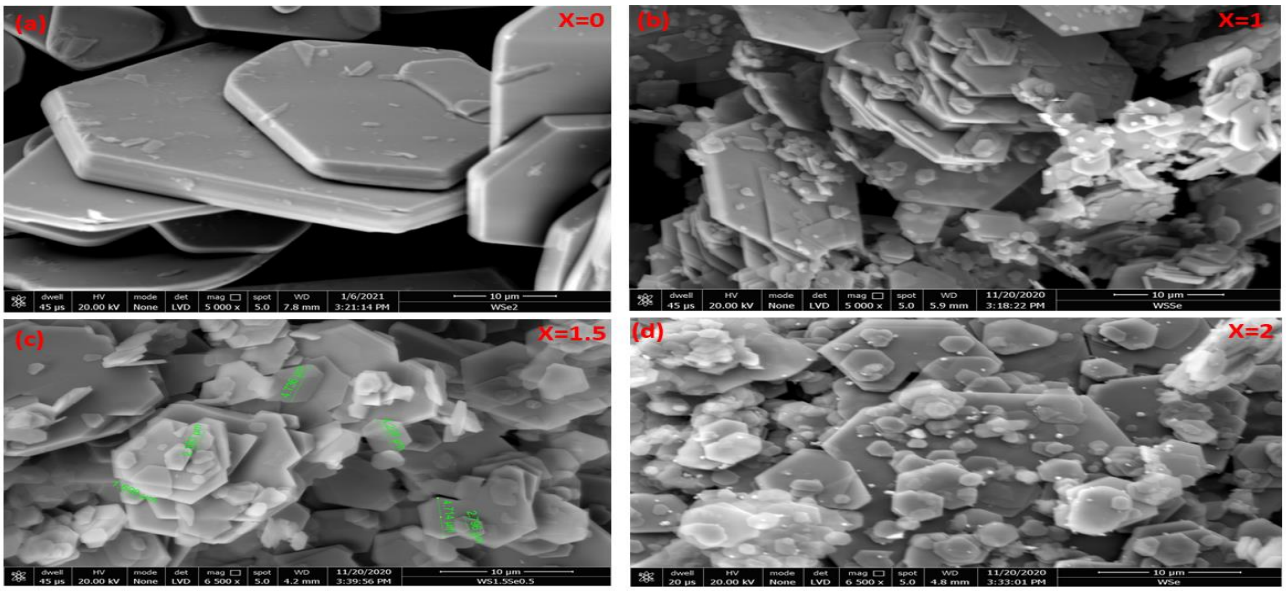

Figure 3. Scanning electron microscope image of WSxSe2-x (x=0.0, 1.0, 1.5, 2.0) SCs.

The comparative study of the PXRD spectra of WS_xSe_{2-x} (x=0.0, 1.0, 1.5, 2.0) SCs is shown in Figure 4. Detected peaks were analyzed by the CHART software to identify the diffracted peaks. From Figure 4 pink color indicated to the spectrum of the WS_2 single crystal and its main peak is detected at 14.34° for (002) plane. In WSe_2, magnified view of the peak associated with (002) plane is located at 13.64° as shown in Figure 4b. It is observed that on incorporation of sulphur in to WSe_2, the (002) prominent peak is shifting from 13.64° to 14.34° as a consequence d-spacing is decreasing from 6.45 Å to 6.17 Å. Due to lattice defects, the Bragg's condition is not satisfied at same angle and hence the unit cell volume is decreased respectively as going from WSe_2 to WS_2. Additionally, the lattice parameters such as macrostrain, crystallite size of grown alloys are also significantly affected due to alloy engineering. Values of lattice parameters are tabulated in Table 1.

Sample	Lattice parameter		c/a	Volume $(Å)^3$	FWHM	2θ (degree)	Crystallinesize t (nm)	Micro strainε x (10^{-3}) $(lin^{-2}\ m^{-4})$	Dislocation density δx10^{15} (lin m^{-4})
	a=b(Å)	c(Å)							
WSe_2	3.29	12.98	3.94	122.06	0.32	13.62	23.3	1.63	2.51
WSSe	3.23	12.68	3.93	114.47	0.47	13.99	13.7	3.55	8.10
$WS_{1.5}Se_{0.5}$	3.21	12.58	3.92	112.14	0.12	14.04	38.3	1.05	0.57
WS_2	3.15	12.32	3.91	105.97	0.45	14.34	17.4	2.10	4.66

Table 1. Structural parameter of WS_xSe_{2-x} (x=0.0, 1.0, 1.5, 2.0) SCs.

 DOI : 10.35291/2454-9150.2023.0200

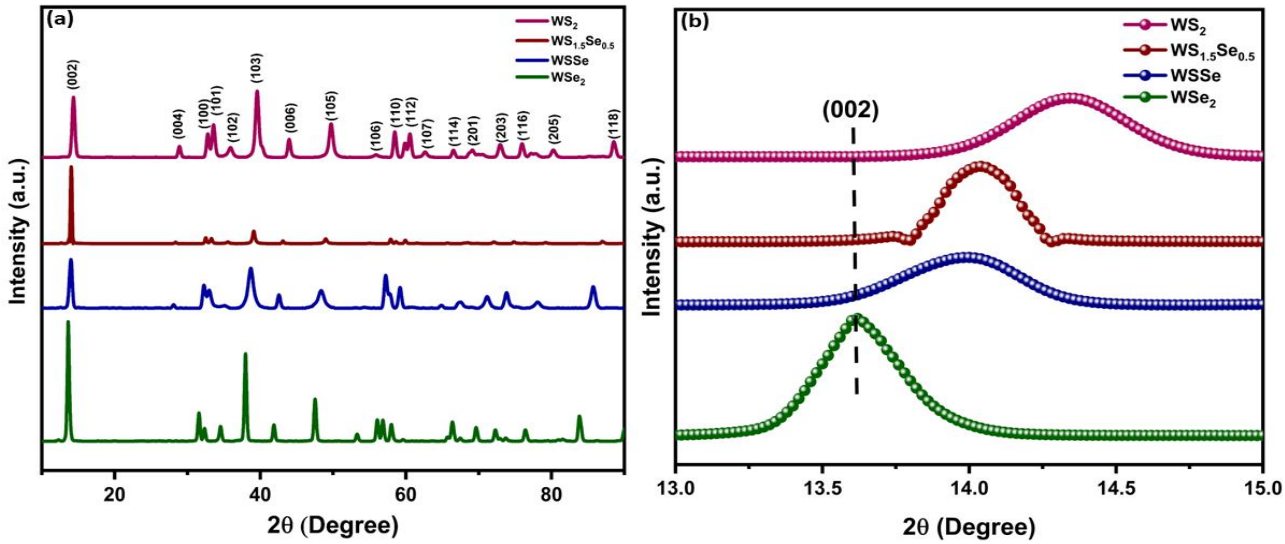

Figure 4. (a) Powder XRD image of WSxSe2-x SCs (b) Magnifying image of (002) plane

High resolution transmission electron microscopy (HRTEM) and selected area electron diffraction (SAED) are useful to identify various information of grown samples at atomic scale such as point defects, dislocation, internal structure authentication and in-depth structural information. Herein, surface texture and crystallinity confirmation of the as-grown WS_xSe_{2-x} (x=0.0, 1.0, 1.5, 2.0) SCs are confirmed by HRTEM and SAED. A suspension for HRTEM was prepared systematically. A powder of grown alloy was placed in acetone and sonicated it for 5 min to release the nano sheets. It was drop casted on Cu grid. This suspension was analyzed by HRTEM as shown in Figure 5(a-d). The images of tiny nano flakes of grown samples are observed by the transmission electron microscope in the range of 200nm to 500nm which is show in Figure 5(a-d). From the magnified view of the nano flakes, it is clearly showing the presence of the planes which are arranged in quasiperiodic manner as shown in Figure 6(a-d). The lattice fringes found to be having 0.645 nm interplanar spacing distance for WSe_2 single crystal that corresponds to prominent pick of (002) plane, similarly d-spacing was observed to be 0.639 nm, 0.625 nm, 0.617 nm for the grown crystals WSSe, $WS_{1.5}Se_{0.5}$, WS_2 respectively as shown in Figure 7 (a-d). The hexagonal spot pattern of grown alloys revealed by SAED displays single crystalline nature as shown in Figure 8 (a-d). In these SAED pattern, planes are also indexed which are in an agreement with PXRD data. Moreover, the spots are found to be (006) plane and its nearest plane was observed to be (118) plane. Similarly, for WSSe crystals spots are observed from the plane which is shown in Figure 8(a-d). Interplanar spacing – d is found between the adjacent fringes of WS_xSe_{2-x} (x=0.0,1.0,1.5,2.0) SCs lattices.

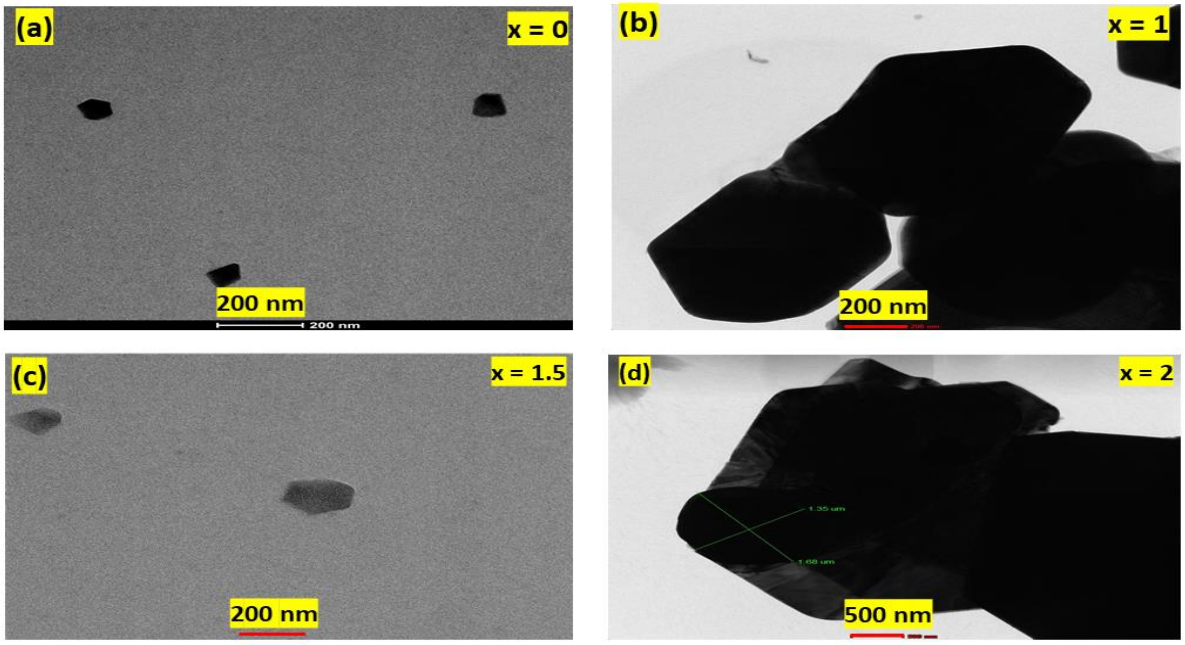

Figure 5. HRTEM image of WSxSe2-x (x=0.0, 1.0, 1.5, 2.0) SCs.

 DOI : 10.35291/2454-9150.2023.0200

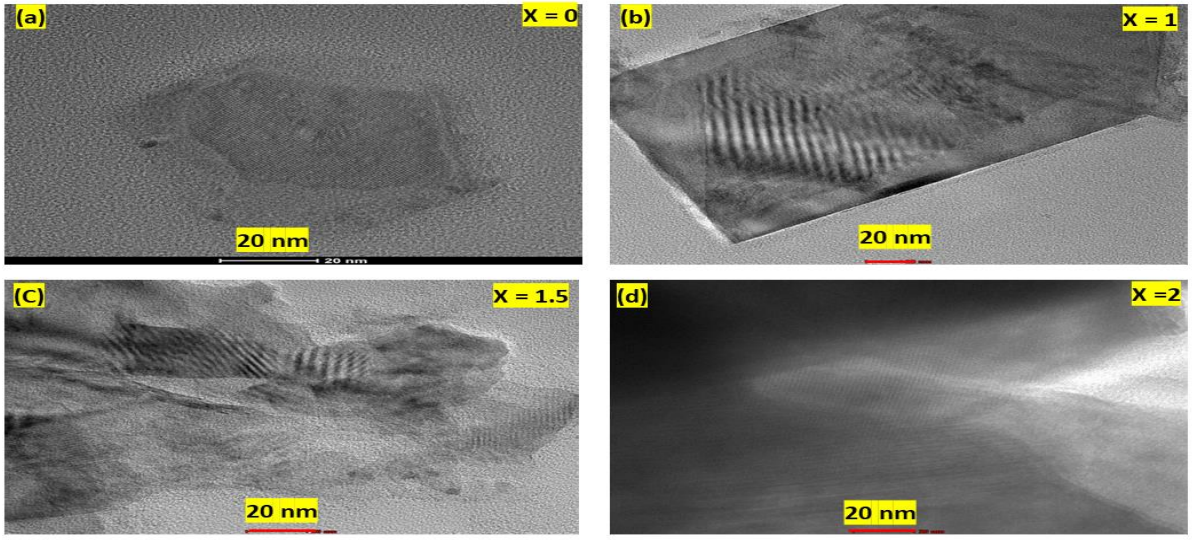

Figure 6. Magnified image of nano flakes of WSxSe2-x (x=0.0, 1.0, 1.5, 2.0) SCs.

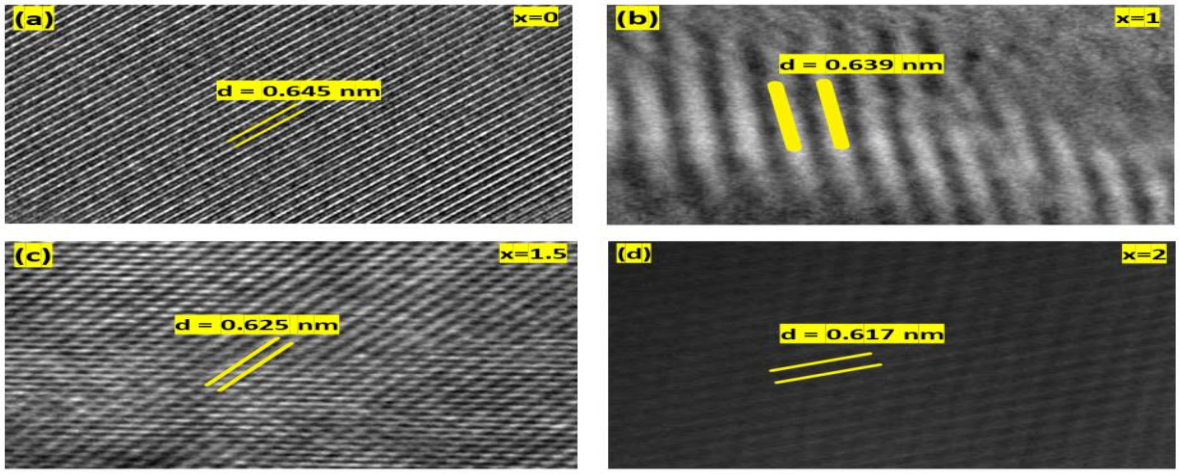

Figure 2.14. Lattice fringes of WS_XSe_{2-x} (x=0.0, 1.0, 1.5, 2.0) SCs.

Figure 7. Lattice fringes of WSxSe2-x (x=0.0, 1.0, 1.5, 2.0) SCs.

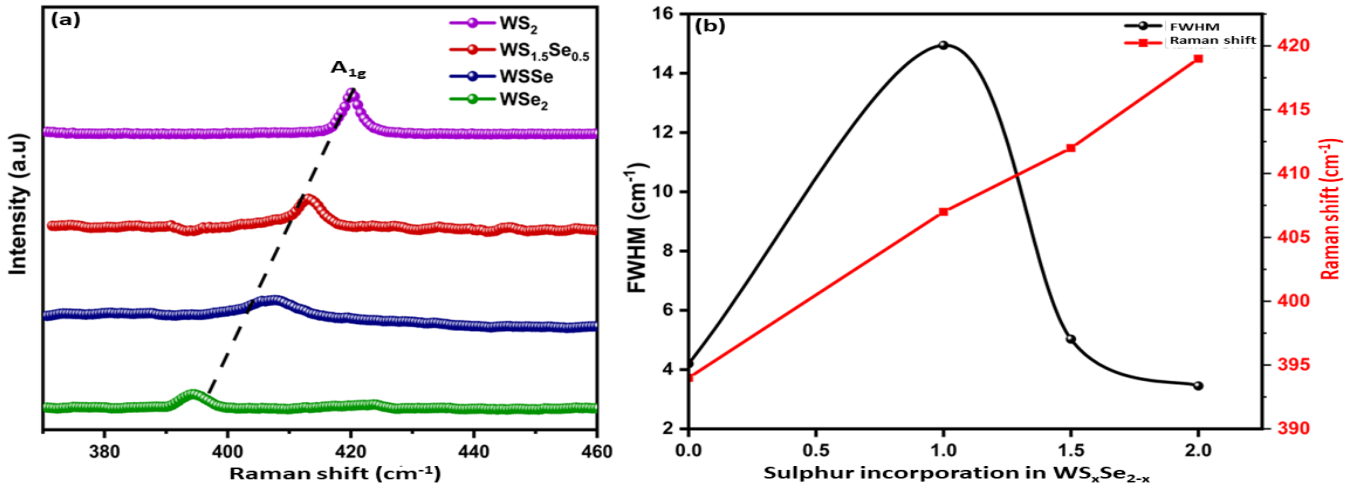

Figure 8. SAED pattern of WSxSe2-x (x=0.0, 1.0, 1.5, 2.0) SCs.

Figure 9(a) shows Raman spectra of WS_xSe_{2-x} (x=0.0,1.0,1.5,2.0) SCs using 785 nm laser source with backscattered geometry. The prominent peak is attributed to the out-of-plane A_{1g} mode allocated at 394.16 cm^{-1} for WSe_2 single crystal. Here the A_{1g} mode was observed due to the out-of-plane vibration. Due to the incorporation of sulphur in WS_xSe_{2-x} (x=0.0, 1.0, 1.5, 2.0) SCs, the bond length and symmetry are changed and hence shifting of A_{1g} mode towards higher frequency is observed as going from WSe_2 to WS_2. Sulphur incorporation affects vibrational modes and shifts Raman peaks significantly. The bond length of WSe_2

 DOI : 10.35291/2454-9150.2023.0200

is larger than WS_2 so it is observed that vibrational peak energy increases with decreasing bond length [19]. Figure 9(b) display the variation in the FWHM (Full Width Half Maximum) and peak position of the A_{1g} mode as a function of sulphur concentration.

Figure 10a. displays the I-V characteristics of the WS_xSe_{2-x} (x = 0.0, 1.0, 1.5, 2.0) photo detectors (PD) under 670 nm LED source. It is found that the current under illumination decreases with the increase in sulphur incorporation. Pulse photo response under different wavelength sources at 1 mV as shown in Figure 10b. The observation of the pulse photocurrent of all PDs portrayed rapid improvement and decay upon switching on and off the light under monochromatic and polychromatic light sources with a fixed illumination intensity of 30 mW/cm^2. It can be seen that the current increases rapidly when the light is turned on. Enhancement in photocurrent upon illumination is attributed to the quick separation of electron-hole pairs due to the absorption of light photons [20]. The photo current under red (670 nm) wavelength illumination is found to be 1.20 µA and 0.40 µA for WSe_2 and WS_2 SC photodetectors respectively. Due to sulphur's high resistance compared to selenium, WS_2's electrical resistance is higher than WSe_2. Therefore, current is facing more path resistance while passing through surface of WS_2 photodetector compared to WSe_2 PD. As a result, photo detection performance of WS_2 based photodetector is lower than WSe_2 based photodetector. Thus, the photocurrent of the WSe_2 detector is found to be gradually decreased as the sulphur concentration was increased. The value of photocurrent of the WSSe, $WS_{1.5}Se_{0.5}$ and WS_2 PDs are 0.97 µA, 0.65 µA, and 0.40 µA respectively. Figure 10c displays the magnified single pulse image of the WSe_2 detector under the red-light source. It can be seen that the rise time and decay time are recorded as 0.372 second and 0.374 second respectively that indicate a faster response of detector. The calculated detector parameters of WS_xSe_{2-x} (x=0.0, 1.0, 1.5, 2.0) SCs photodetectors are shown in

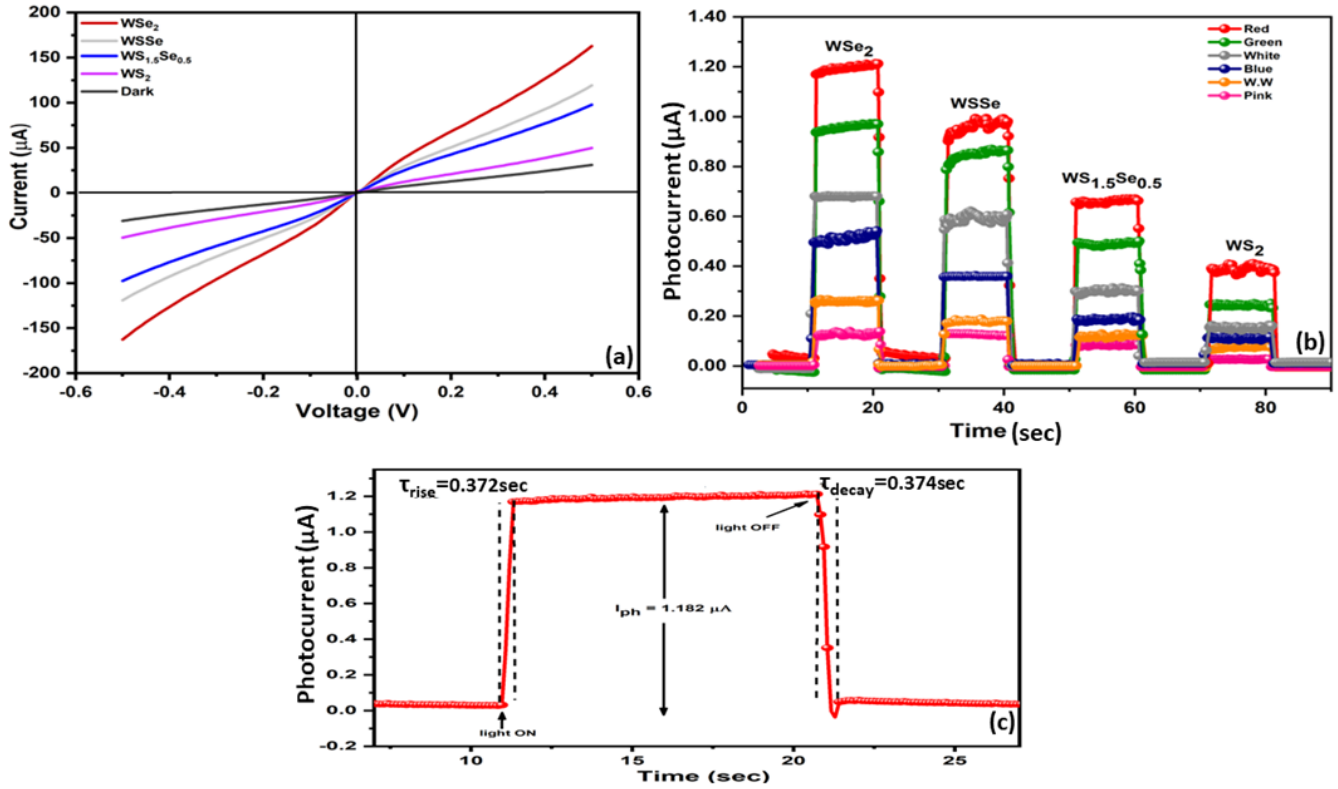

Figure 9. (a) Raman spectra of WSxSe2-x (x=0.0, 1.0, 1.5, 2.0) (b) Variation of FWHM and Raman sift of the WSxSe2-x SCs under 785 nm laser source.

Figure 10. (a) I-V characteristics of WSxSe2-x (x= 0.0, 1.0, 1.5, 2.0) SCs (b) Pulse photo response of WSxSe2-x (x= 0.0, 1.0, 1.5, 2.0) SCs (c) Single pulse for WSe2 PD.

Table 2. **. pulse photo response parameter of WS_xSe_{2-x} (x= 0.0, 1.0, 1.5, 2.0) under 670nm illumination.**

Photodetector	Rise time(s)	Decay time(s)	I_{ph} (µA)	Responsivity (mAW^{-1})	Detectivity (Jones) $x10^9$
WSe_2	0.372	0.374	1.182	0.315	2.792
WSSe	0.376	0.375	0.981	0.261	2.312
$WS_{1.5}Se_{0.5}$	0.426	0.428	0.638	0.168	1.494
WS_2	0.432	0.434	0.382	0.101	0.896

 DOI : 10.35291/2454-9150.2023.0200

IV. CONCLUSION

In summary, we have shown that WS_xSe_{2-x} (x=0.0, 1.0, 1.5, 2.0) SCs are grown by direct vapour transport technique. There is no extra peak in the EDAX spectrum. SEM and optical microscopy showed that the crystals have hexagonal lattice structures. The crystallinity structure of the grown alloy was revealed by SAED and XRD. The HRTEM analysis revealed that the alloy contained nanoflakes as well as a hexagonal internal structure. Based on Raman spectroscopy, A_{1g} mode is shown to have an out-of-plan vibrational mode, and due to the amount of sulphur in corporation in WSe_2 ternary alloy, Raman peaks are shifting towards higher frequency. WS_xSe_{2-x} (x=0.0, 1.0, 1.5, 2.0) single crystals fabricated as switchable photo response mechanisms show high photoresponsivity and detectability. Here photoresponsivity is increased with decreasing sulphur substitution in WS_xSe_{2-x} (x=0.0, 1.0, 1.5, 2.0) ternary alloy. Among all the detectors, the WSe_2 photodetector demonstrated superior photo response compared to other detectors. The photodetector represents a rapid pulse photo response. Therefore, this high performance indicates that a high photocurrent of 1.20 μA is found in the visible region, especially in the 670 nm region.

REFERENCES

[1] Gupta, S. U.; Dalvaniya, A. G.; Chauhan, P.; Patel, K. D.; Solanki, G. K.; Pathak, V. M.; Jha, P. K. Cryotronic Low-Powered Strained Polymorphic Photodetector Functionalized by Palladium Incorporated Tin Diselenide. Advanced Optical Materials **2022**, 10 (20), 1–11.

[2] Gupta, S. U.; Dalvaniya, A. G.; Patel, N. F.; Bhakhar, S. A.; Nair, S.; Joy, J.; Patel, K. D.; Solanki, G. K.; Pathak, V. M.; Som, N. N.; Jha, P. K.; Panda, D. K. Optical Switching Device Based on a Crystalline $SnSe_2$ Photodetector in Diverse Conditions . ACS Applied Electronic Materials **2021**.

[3] Gupta, S. U.; Dalvaniya, A. G.; Limberkar, C.; Patel, K. D.; Solanki, G. K.; Pathak, V. M.; Pataniya, P. M.; Sumesh, C. K.; Som, N. N.; Jha, P. K.; Patel, V. Annealing Induced Phase Transformation from Amorphous to Polycrystalline $SnSe_2$ Thin Film Photo Detector with Enhanced Light-Matter Interaction. Journal of Non-Crystalline Solids **2022**, 578 (December 2021), 121353.

[4] Pawar, M. S.; Kadam, S. R.; Kale, B. B.; Late, D. J. $MoS_2$and $CdMoS_4$nanostructure-Based UV Light Photodetectors. *Nanoscale Advances* **2021**, *3* (16), 4799–4803.

[5] Tsai, C. Y.; Tai, H. C.; Su, C. A.; Chiang, L. M.; Li, Y. Y. Activated Microporous Carbon Nanospheres for Use in Supercapacitors. ACS Applied Nano Materials **2020**, 3 (10), 10380–10388..

[6] Carvalho, T. C. V.; Araujo, F. D. V.; Costa Dos Santos, C.; Alencar, L. M. R.; Ribeiro-Soares, J.; Late, D. J.; Lobo, A. O.; Souza Filho, A. G.; Alencar, R. S.; Viana, B. C. Temperature-Dependent Phonon Dynamics of Supported and Suspended Monolayer Tungsten Diselenide. AIP Advances **2019**, 9 (8).

[7] Pataniya, P. M.; Tannarana, M.; Zankat, C. K.; Bhakhar, S. A.; Narayan, S.; Solanki, G. K.; Patel, K. D.; Jha, P. K.; Pathak, V. M. Low-Temperature Raman Investigations and Photoresponse of a Detector Based on High-Quality WSe_2 Crystals. *Journal of Physical Chemistry C* **2020**, *124* (4), 2251–2257.

[8] Patel, N. F.; Bhakhar, S. A.; Solanki, G. K.; Patel, K. D.; Pathak, V. M.; Zankat, C. K.; Pataniya, P. M.; Gohil, J. D.; Gupta, S. U. Sonochemical Exfoliation, Characterization and Photoresponse of $MoS_{0.5}Se_{1.5}$ Nanosheets. *Journal of Materials Science: Materials in Electronics* **2021**, *32* (9), 11805–11812.

[9] Pataniya, P.; Zankat, C. K.; Tannarana, M.; Kesav, C. Paper Based Flexible Photodetector Functionalized by WSe_2 Nanodots. **2019**.

[10] Pham, T.; Li, G.; Bekyarova, E.; Itkis, M. E.; Mulchandani, A. MoS 2 -Based Optoelectronic Gas Sensor with Sub-Parts-per-Billion Limit of NO 2 Gas Detection. *ACS Nano* **2019**, *13* (3), 3196–3205.

[11] Li, S.; Zhang, Y.; Yang, W.; Liu, H.; Fang, X. 2D Perovskite Sr2Nb3O10 for High-Performance UV Photodetectors. *Advanced Materials* **2020**, *32* (7), 1–10.

[12] Dalvaniya, A. G.; Gupta, S. U.; Patel, K. D.; Solanki, G. K.; Pathak, V. M. Superior Cryotronics Performance of the In/p-WS_2 Schottky Interface . ACS Applied Electronic Materials **2022**.

[13] Taghavi, N. S.; Gant, P.; Huang, P.; Niehues, I.; Schmidt, R.; Michaelis de Vasconcellos, S.; Bratschitsch, R.; García-Hernández, M.; Frisenda, R.; Castellanos-Gomez, A. Thickness Determination of MoS2, MoSe2, WS2 and WSe2 on Transparent Stamps Used for Deterministic Transfer of 2D Materials. *Nano Research* **2019**, *12* (7), 1691–1695.

[14] Zhang, Y.; Li, S.; Li, Z.; Liu, H.; Liu, X.; Chen, J.; Fang, X. High-Performance Two-Dimensional Perovskite Ca2Nb3O10 UV Photodetectors. *Nano Letters* **2021**, *21* (1), 382–388.

[15] Huang, L.; Dong, B.; Guo, X.; Chang, Y.; Chen, N.; Huang, X.; Liao, W.; Zhu, C.; Wang, H.; Lee, C.; Ang, K. W. Waveguide-Integrated Black Phosphorus Photodetector for Mid-Infrared Applications. ACS Nano **2019**, 13 (1), 913–921.

[16] Sumesh, C. K.; Kapatel, S.; Chaudhari, A. An Approach for Scalable Production of Silver (Ag) Decorated WS_2 Nanosheets. AIP Conf. Proc. **2018**, 1961.

[17] Van de Voorde, M.; Duchemin, C.; Heinke, R.; Lambert, L.; Chevallay, E.; Schneider, T.; Van Stenis, M.; Cocolios, T. E.; Cardinaels, T.; Ponsard, B.; Ooms, M.; Stora, T.; Burgoyne, A. R. Production of Sm-153 With Very High Specific Activity for Targeted Radionuclide Therapy. Front. Med. **2021**, 8 (July), 1–9.

[18] Kannaujiya, R. M.; Khimani, A. J.; Chaki, S. H.; Chauhan, S. M.; Hirpara, A. B.; Deshpande, M. P. Growth and Characterizations of Tin Telluride (SnTe) Single Crystals. Eur. Phys. J. Plus **2020**, 135 (1), 1–12.

[19] Tannarana, M.; Pataniya, P.; Solanki, G. K.; Bhakhar, S. A.; Narayan, S.; Patel, K. D.; Jha, P. K.; Pathak, V. M. Temperature-Dependent Vibrational Properties of $Sb_xSn_{1-x}Se_2$ (x = 0, 0.1, 0.2 & 0.3) Ternary Alloys. Eur. Phys. J. Plus **2020**, 135 (1), 1–7.

[20] Zankat, C. K.; Pataniya, P.; Tannarana, M.; Solanki, G. K.; Patel, K. D.; Pathak, V. M. Promoting Photoresponse of Resistive Detector Based on $V_{0.15}Sn_{0.85}Se_2$ Ternary Alloy. Mater. Sci. Semicond. Process. **2019**, 91 (December 2018), 383–386.

 DOI : 10.35291/2454-9150.2023.0200